Study of the decay $D^+ \to K^*(892)^+ K_S^0$ in $D^+ \to K^+ K_S^0 \pi^0$

M. Ablikim,[1] M. N. Achasov,[10,c] P. Adlarson,[67] S. Ahmed,[15] M. Albrecht,[4] R. Aliberti,[28] A. Amoroso,[66a,66c] M. R. An,[32] Q. An,[63,49] X. H. Bai,[57] Y. Bai,[48] O. Bakina,[29] R. Baldini Ferroli,[23a] I. Balossino,[24a] Y. Ban,[38,k] K. Begzsuren,[26] N. Berger,[28] M. Bertani,[23a] D. Bettoni,[24a] F. Bianchi,[66a,66c] J. Bloms,[60] A. Bortone,[66a,66c] I. Boyko,[29] R. A. Briere,[5] H. Cai,[68] X. Cai,[1,49] A. Calcaterra,[23a] G. F. Cao,[1,54] N. Cao,[1,54] S. A. Cetin,[53a] J. F. Chang,[1,49] W. L. Chang,[1,54] G. Chelkov,[29,b] D. Y. Chen,[6] G. Chen,[1] H. S. Chen,[1,54] M. L. Chen,[1,49] S. J. Chen,[35] X. R. Chen,[25] Y. B. Chen,[1,49] Z. J. Chen,[20,l] W. S. Cheng,[66c] G. Cibinetto,[24a] F. Cossio,[66c] X. F. Cui,[36] H. L. Dai,[1,49] X. C. Dai,[1,54] A. Dbeyssi,[15] R. E. de Boer,[4] D. Dedovich,[29] Z. Y. Deng,[1] A. Denig,[28] I. Denysenko,[29] M. Destefanis,[66a,66c] F. De Mori,[66a,66c] Y. Ding,[33] C. Dong,[36] J. Dong,[1,49] L. Y. Dong,[1,54] M. Y. Dong,[1,49,54] X. Dong,[68] S. X. Du,[71] Y. L. Fan,[68] J. Fang,[1,49] S. S. Fang,[1,54] Y. Fang,[1] R. Farinelli,[24a] L. Fava,[66b,66c] F. Feldbauer,[4] G. Felici,[23a] C. Q. Feng,[63,49] J. H. Feng,[50] M. Fritsch,[4] C. D. Fu,[1] Y. Gao,[63,49] Y. Gao,[38,k] Y. Gao,[64] Y. G. Gao,[6] I. Garzia,[24a,24b] P. T. Ge,[68] C. Geng,[50] E. M. Gersabeck,[58] A. Gilman,[61] K. Goetzen,[11] L. Gong,[33] W. X. Gong,[1,49] W. Gradl,[28] M. Greco,[66a,66c] L. M. Gu,[35] M. H. Gu,[1,49] S. Gu,[2] Y. T. Gu,[13] C. Y. Guan,[1,54] A. Q. Guo,[22] L. B. Guo,[34] R. P. Guo,[40] Y. P. Guo,[9,h] A. Guskov,[29] T. T. Han,[41] W. Y. Han,[32] X. Q. Hao,[16] F. A. Harris,[56] N. Hüsken,[22,28] K. L. He,[1,54] F. H. Heinsius,[4] C. H. Heinz,[28] T. Held,[4] Y. K. Heng,[1,49,54] C. Herold,[51] M. Himmelreich,[11,f] T. Holtmann,[4] G. Y. Hou,[1,54] Y. R. Hou,[54] Z. L. Hou,[1] H. M. Hu,[1,54] J. F. Hu,[47,m] T. Hu,[1,49,54] Y. Hu,[1] G. S. Huang,[63,49] L. Q. Huang,[64] X. T. Huang,[41] Y. P. Huang,[1] Z. Huang,[38,k] T. Hussain,[65] W. Ikegami Andersson,[67] W. Imoehl,[22] M. Irshad,[63,49] S. Jaeger,[4] S. Janchiv,[26,j] Q. Ji,[1] Q. P. Ji,[16] X. B. Ji,[1,54] X. L. Ji,[1,49] Y. Y. Ji,[41] H. B. Jiang,[41] X. S. Jiang,[1,49,54] J. B. Jiao,[41] Z. Jiao,[18] S. Jin,[35] Y. Jin,[57] M. Q. Jing,[1,54] T. Johansson,[67] N. Kalantar-Nayestanaki,[55] X. S. Kang,[33] R. Kappert,[55] M. Kavatsyuk,[55] B. C. Ke,[43,1] I. K. Keshk,[4] A. Khoukaz,[60] P. Kiese,[28] R. Kiuchi,[1] R. Kliemt,[11] L. Koch,[30] O. B. Kolcu,[53a,e] B. Kopf,[4] M. Kuemmel,[4] M. Kuessner,[4] A. Kupsc,[67] M. G. Kurth,[1,54] W. Kühn,[30] J. J. Lane,[58] J. S. Lange,[30] P. Larin,[15] A. Lavania,[21] L. Lavezzi,[66a,66c] Z. H. Lei,[63,49] H. Leithoff,[28] M. Lellmann,[28] T. Lenz,[28] C. Li,[39] C. H. Li,[32] Cheng Li,[63,49] D. M. Li,[71] F. Li,[1,49] G. Li,[1] H. Li,[63,49] H. Li,[43] H. B. Li,[1,54] H. J. Li,[16] J. L. Li,[41] J. Q. Li,[4] J. S. Li,[50] Ke Li,[1] L. K. Li,[1] Lei Li,[3] P. R. Li,[31] S. Y. Li,[52] W. D. Li,[1,54] W. G. Li,[1] X. H. Li,[63,49] X. L. Li,[41] Xiaoyu Li,[1,54] Z. Y. Li,[50] H. Liang,[1,54] H. Liang,[63,49] H. Liang,[27] Y. F. Liang,[45] Y. T. Liang,[25] G. R. Liao,[12] L. Z. Liao,[1,54] J. Libby,[21] C. X. Lin,[50] B. J. Liu,[1] C. X. Liu,[1] D. Liu,[15,63] F. H. Liu,[44] Fang Liu,[1] Feng Liu,[6] H. B. Liu,[13] H. M. Liu,[1,54] Huanhuan Liu,[1] Huihui Liu,[17] J. B. Liu,[63,49] J. L. Liu,[64] J. Y. Liu,[1,54] K. Liu,[1] K. Y. Liu,[33] L. Liu,[63,49] M. H. Liu,[9,h] P. L. Liu,[1] Q. Liu,[54] Q. Liu,[68] S. B. Liu,[63,49] Shuai Liu,[46] T. Liu,[1,54] W. M. Liu,[63,49] X. Liu,[31] Y. Liu,[31] Y. B. Liu,[36] Z. A. Liu,[1,49,54] Z. Q. Liu,[41] X. C. Lou,[1,49,54] F. X. Lu,[50] H. J. Lu,[18] J. D. Lu,[1,54] J. G. Lu,[1,49] X. L. Lu,[1] Y. Lu,[1] Y. P. Lu,[1,49] C. L. Luo,[34] M. X. Luo,[70] P. W. Luo,[50] T. Luo,[9,h] X. L. Luo,[1,49] X. R. Lyu,[54] F. C. Ma,[33] H. L. Ma,[1] L. L. Ma,[41] M. M. Ma,[1,54] Q. M. Ma,[1] R. Q. Ma,[1,54] R. T. Ma,[54] X. X. Ma,[1,54] X. Y. Ma,[1,49] F. E. Maas,[15] M. Maggiora,[66a,66c] S. Maldaner,[4] S. Malde,[61] Q. A. Malik,[65] A. Mangoni,[23b] Y. J. Mao,[38,k] Z. P. Mao,[1] S. Marcello,[66a,66c] Z. X. Meng,[57] J. G. Messchendorp,[55] G. Mezzadri,[24a] T. J. Min,[35] R. E. Mitchell,[22] X. H. Mo,[1,49,54] Y. J. Mo,[6] N. Yu. Muchnoi,[10,c] H. Muramatsu,[59] S. Nakhoul,[11,f] Y. Nefedov,[29] F. Nerling,[11,f] I. B. Nikolaev,[10,c] Z. Ning,[1,49] S. Nisar,[8,i] S. L. Olsen,[54] Q. Ouyang,[1,49,54] S. Pacetti,[23b,23c] X. Pan,[9,h] Y. Pan,[58] A. Pathak,[1] P. Patteri,[23a] M. Pelizaeus,[4] H. P. Peng,[63,49] K. Peters,[11,f] J. Pettersson,[67] J. L. Ping,[34] R. G. Ping,[1,54] R. Poling,[59] V. Prasad,[63,49] H. Qi,[63,49] H. R. Qi,[52] K. H. Qi,[25] M. Qi,[35] T. Y. Qi,[9] S. Qian,[1,49] W. B. Qian,[54] Z. Qian,[50] C. F. Qiao,[54] L. Q. Qin,[12] X. P. Qin,[9] X. S. Qin,[41] Z. H. Qin,[1,49] J. F. Qiu,[1] S. Q. Qu,[36] K. H. Rashid,[65] K. Ravindran,[21] C. F. Redmer,[28] A. Rivetti,[66c] V. Rodin,[55] M. Rolo,[66c] G. Rong,[1,54] Ch. Rosner,[15] M. Rump,[60] H. S. Sang,[63] A. Sarantsev,[29,d] Y. Schelhaas,[28] C. Schnier,[4] K. Schoenning,[67] M. Scodeggio,[24a,24b] D. C. Shan,[46] W. Shan,[19] X. Y. Shan,[63,49] J. F. Shangguan,[46] M. Shao,[63,49] C. P. Shen,[9] H. F. Shen,[1,54] P. X. Shen,[36] X. Y. Shen,[1,54] H. C. Shi,[63,49] R. S. Shi,[1,54] X. Shi,[1,49] X. D. Shi,[63,49] J. J. Song,[41] W. M. Song,[27,1] Y. X. Song,[38,k] S. Sosio,[66a,66c] S. Spataro,[66a,66c] K. X. Su,[68] P. P. Su,[46] F. F. Sui,[41] G. X. Sun,[1] H. K. Sun,[1] J. F. Sun,[16] L. Sun,[68] S. S. Sun,[1,54] T. Sun,[1,54] W. Y. Sun,[27] W. Y. Sun,[34] X. Sun,[20,l] Y. J. Sun,[63,49] Y. K. Sun,[63,49] Y. Z. Sun,[1] Z. T. Sun,[1] Y. H. Tan,[68] Y. X. Tan,[63,49] C. J. Tang,[45] G. Y. Tang,[1] J. Tang,[50] J. X. Teng,[63,49] V. Thoren,[67] W. H. Tian,[43] Y. T. Tian,[25] I. Uman,[53b] B. Wang,[1] C. W. Wang,[35] D. Y. Wang,[38,k] H. J. Wang,[31] H. P. Wang,[1,54] K. Wang,[1,49] L. L. Wang,[1] M. Wang,[41] M. Z. Wang,[38,k] Meng Wang,[1,54] W. Wang,[50] W. H. Wang,[68] W. P. Wang,[63,49] X. Wang,[38,k] X. F. Wang,[31] X. L. Wang,[9,h] Y. Wang,[50] Y. Wang,[63,49] Y. D. Wang,[37] Y. F. Wang,[1,49,54] Y. Q. Wang,[1] Y. Y. Wang,[31] Z. Wang,[1,49] Z. Y. Wang,[1] Ziyi Wang,[54] Zongyuan Wang,[1,54] D. H. Wei,[12] F. Weidner,[60] S. P. Wen,[1] D. J. White,[58] U. Wiedner,[4] G. Wilkinson,[61] M. Wolke,[67] L. Wollenberg,[4] J. F. Wu,[1,54] L. H. Wu,[1] L. J. Wu,[1,54] X. Wu,[9,h] Z. Wu,[1,49] L. Xia,[63,49] H. Xiao,[9,h] S. Y. Xiao,[1] Z. J. Xiao,[34] X. H. Xie,[38,k] Y. G. Xie,[1,49] Y. H. Xie,[6] T. Y. Xing,[1,54] G. F. Xu,[1] Q. J. Xu,[14] W. Xu,[1,54] X. P. Xu,[46] Y. C. Xu,[54] F. Yan,[9,h] L. Yan,[9,h] W. B. Yan,[63,49] W. C. Yan,[71] Xu Yan,[46] H. J. Yang,[42,g] H. X. Yang,[1] L. Yang,[43] S. L. Yang,[54] Y. X. Yang,[12] Yifan Yang,[1,54] Zhi Yang,[25] M. Ye,[1,49] M. H. Ye,[7] J. H. Yin,[1] Z. Y. You,[50] B. X. Yu,[1,49,54] C. X. Yu,[36] G. Yu,[1,54] J. S. Yu,[20,l] T. Yu,[64] C. Z. Yuan,[1,54] L. Yuan,[2] X. Q. Yuan,[38,k] Y. Yuan,[1] Z. Y. Yuan,[50] C. X. Yue,[32] A. Yuncu,[53a,a] A. A. Zafar,[65] X. Zeng,[6] Y. Zeng,[20,l] A. Q. Zhang,[1] B. X. Zhang,[1] Guangyi Zhang,[16] H. Zhang,[63] H. H. Zhang,[27] H. H. Zhang,[50] H. Y. Zhang,[1,49]

J. J. Zhang,[43] J. L. Zhang,[69] J. Q. Zhang,[34] J. W. Zhang,[1,49,54] J. Y. Zhang,[1] J. Z. Zhang,[1,54] Jianyu Zhang,[1,54] Jiawei Zhang,[1,54] L. M. Zhang,[52] L. Q. Zhang,[50] Lei Zhang,[35] S. Zhang,[50] S. F. Zhang,[35] Shulei Zhang,[20,l] X. D. Zhang,[37] X. Y. Zhang,[41] Y. Zhang,[61] Y. H. Zhang,[1,49] Y. T. Zhang,[63,49] Yan Zhang,[63,49] Yao Zhang,[1] Yi Zhang,[9,h] Z. H. Zhang,[6] Z. Y. Zhang,[68] G. Zhao,[1] J. Zhao,[32] J. Y. Zhao,[1,54] J. Z. Zhao,[1,49] Lei Zhao,[63,49] Ling Zhao,[1] M. G. Zhao,[36] Q. Zhao,[1] S. J. Zhao,[71] Y. B. Zhao,[1,49] Y. X. Zhao,[25] Z. G. Zhao,[63,49] A. Zhemchugov,[29,b] B. Zheng,[64] J. P. Zheng,[1,49] Y. Zheng,[38,k] Y. H. Zheng,[54] B. Zhong,[34] C. Zhong,[64] L. P. Zhou,[1,54] Q. Zhou,[1,54] X. Zhou,[68] X. K. Zhou,[54] X. R. Zhou,[63,49] X. Y. Zhou,[32] A. N. Zhu,[1,54] J. Zhu,[36] K. Zhu,[1] K. J. Zhu,[1,49,54] S. H. Zhu,[62] T. J. Zhu,[69] W. J. Zhu,[9,h] W. J. Zhu,[36] Y. C. Zhu,[63,49] Z. A. Zhu,[1,54] B. S. Zou,[1] and J. H. Zou[1]

(BESIII Collaboration)

[1]*Institute of High Energy Physics, Beijing 100049, People's Republic of China*
[2]*Beihang University, Beijing 100191, People's Republic of China*
[3]*Beijing Institute of Petrochemical Technology, Beijing 102617, People's Republic of China*
[4]*Bochum Ruhr-University, D-44780 Bochum, Germany*
[5]*Carnegie Mellon University, Pittsburgh, Pennsylvania 15213, USA*
[6]*Central China Normal University, Wuhan 430079, People's Republic of China*
[7]*China Center of Advanced Science and Technology, Beijing 100190, People's Republic of China*
[8]*COMSATS University Islamabad, Lahore Campus, Defence Road, Off Raiwind Road,*
54000 Lahore, Pakistan
[9]*Fudan University, Shanghai 200443, People's Republic of China*
[10]*G.I. Budker Institute of Nuclear Physics SB RAS (BINP), Novosibirsk 630090, Russia*
[11]*GSI Helmholtzcentre for Heavy Ion Research GmbH, D-64291 Darmstadt, Germany*
[12]*Guangxi Normal University, Guilin 541004, People's Republic of China*
[13]*Guangxi University, Nanning 530004, People's Republic of China*
[14]*Hangzhou Normal University, Hangzhou 310036, People's Republic of China*
[15]*Helmholtz Institute Mainz, Staudinger Weg 18, D-55099 Mainz, Germany*
[16]*Henan Normal University, Xinxiang 453007, People's Republic of China*
[17]*Henan University of Science and Technology, Luoyang 471003, People's Republic of China*
[18]*Huangshan College, Huangshan 245000, People's Republic of China*
[19]*Hunan Normal University, Changsha 410081, People's Republic of China*
[20]*Hunan University, Changsha 410082, People's Republic of China*
[21]*Indian Institute of Technology Madras, Chennai 600036, India*
[22]*Indiana University, Bloomington, Indiana 47405, USA*
[23a]*INFN Laboratori Nazionali di Frascati, I-00044, Frascati, Italy*
[23b]*INFN Sezione di Perugia, I-06100, Perugia, Italy*
[23c]*University of Perugia, I-06100, Perugia, Italy*
[24a]*INFN Sezione di Ferrara, I-44122, Ferrara, Italy*
[24b]*University of Ferrara, I-44122, Ferrara, Italy*
[25]*Institute of Modern Physics, Lanzhou 730000, People's Republic of China*
[26]*Institute of Physics and Technology, Peace Ave. 54B, Ulaanbaatar 13330, Mongolia*
[27]*Jilin University, Changchun 130012, People's Republic of China*
[28]*Johannes Gutenberg University of Mainz, Johann-Joachim-Becher-Weg 45, D-55099 Mainz, Germany*
[29]*Joint Institute for Nuclear Research, 141980 Dubna, Moscow region, Russia*
[30]*Justus-Liebig-Universitaet Giessen, II. Physikalisches Institut, Heinrich-Buff-Ring 16,*
D-35392 Giessen, Germany
[31]*Lanzhou University, Lanzhou 730000, People's Republic of China*
[32]*Liaoning Normal University, Dalian 116029, People's Republic of China*
[33]*Liaoning University, Shenyang 110036, People's Republic of China*
[34]*Nanjing Normal University, Nanjing 210023, People's Republic of China*
[35]*Nanjing University, Nanjing 210093, People's Republic of China*
[36]*Nankai University, Tianjin 300071, People's Republic of China*
[37]*North China Electric Power University, Beijing 102206, People's Republic of China*
[38]*Peking University, Beijing 100871, People's Republic of China*
[39]*Qufu Normal University, Qufu 273165, People's Republic of China*
[40]*Shandong Normal University, Jinan 250014, People's Republic of China*
[41]*Shandong University, Jinan 250100, People's Republic of China*
[42]*Shanghai Jiao Tong University, Shanghai 200240, People's Republic of China*
[43]*Shanxi Normal University, Linfen 041004, People's Republic of China*

[44]Shanxi University, Taiyuan 030006, People's Republic of China
[45]Sichuan University, Chengdu 610064, People's Republic of China
[46]Soochow University, Suzhou 215006, People's Republic of China
[47]South China Normal University, Guangzhou 510006, People's Republic of China
[48]Southeast University, Nanjing 211100, People's Republic of China
[49]State Key Laboratory of Particle Detection and Electronics,
Beijing 100049, Hefei 230026, People's Republic of China
[50]Sun Yat-Sen University, Guangzhou 510275, People's Republic of China
[51]Suranaree University of Technology, University Avenue 111, Nakhon Ratchasima 30000, Thailand
[52]Tsinghua University, Beijing 100084, People's Republic of China
[53a]Turkish Accelerator Center Particle Factory Group,
Istanbul Bilgi University, 34060 Eyup, Istanbul, Turkey
[53b]Near East University, Nicosia, North Cyprus, Mersin 10, Turkey
[54]University of Chinese Academy of Sciences, Beijing 100049, People's Republic of China
[55]University of Groningen, NL-9747 AA Groningen, The Netherlands
[56]University of Hawaii, Honolulu, Hawaii 96822, USA
[57]University of Jinan, Jinan 250022, People's Republic of China
[58]University of Manchester, Oxford Road, Manchester, M13 9PL, United Kingdom
[59]University of Minnesota, Minneapolis, Minnesota 55455, USA
[60]University of Muenster, Wilhelm-Klemm-Str. 9, 48149 Muenster, Germany
[61]University of Oxford, Keble Rd, Oxford, United Kingdom OX13RH
[62]University of Science and Technology Liaoning, Anshan 114051, People's Republic of China
[63]University of Science and Technology of China, Hefei 230026, People's Republic of China
[64]University of South China, Hengyang 421001, People's Republic of China
[65]University of the Punjab, Lahore-54590, Pakistan
[66a]University of Turin and INFN, University of Turin, I-10125, Turin, Italy
[66b]University of Eastern Piedmont, I-15121, Alessandria, Italy
[66c]INFN, I-10125, Turin, Italy
[67]Uppsala University, Box 516, SE-75120 Uppsala, Sweden
[68]Wuhan University, Wuhan 430072, People's Republic of China
[69]Xinyang Normal University, Xinyang 464000, People's Republic of China
[70]Zhejiang University, Hangzhou 310027, People's Republic of China
[71]Zhengzhou University, Zhengzhou 450001, People's Republic of China

Based on an e^+e^- collision data sample corresponding to an integrated luminosity of 2.93 fb^{-1} collected with the BESIII detector at $\sqrt{s} = 3.773$ GeV, the first amplitude analysis of the singly Cabibbo-suppressed decay $D^+ \rightarrow K^+ K_S^0 \pi^0$ is performed. From the amplitude analysis, the $K^*(892)^+ K_S^0$ component is found to be dominant with a fraction of $(57.1 \pm 2.6 \pm 4.2)\%$, where the first uncertainty is statistical and the second

[a]Also at Bogazici University, 34342 Istanbul, Turkey.
[b]Also at the Moscow Institute of Physics and Technology, Moscow 141700, Russia.
[c]Also at the Novosibirsk State University, Novosibirsk, 630090, Russia.
[d]Also at the NRC "Kurchatov Institute," PNPI, 188300, Gatchina, Russia.
[e]Also at Istanbul Arel University, 34295 Istanbul, Turkey.
[f]Also at Goethe University Frankfurt, 60323 Frankfurt am Main, Germany.
[g]Also at Key Laboratory for Particle Physics, Astrophysics and Cosmology, Ministry of Education; Shanghai Key Laboratory for Particle Physics and Cosmology; Institute of Nuclear and Particle Physics, Shanghai 200240, People's Republic of China.
[h]Also at Key Laboratory of Nuclear Physics and Ion-beam Application (MOE) and Institute of Modern Physics, Fudan University, Shanghai 200443, People's Republic of China.
[i]Also at Harvard University, Department of Physics, Cambridge, Massachusetts 02138, USA.
[j]Currently at: Institute of Physics and Technology, Peace Ave. 54B, Ulaanbaatar 13330, Mongolia.
[k]Also at State Key Laboratory of Nuclear Physics and Technology, Peking University, Beijing 100871, People's Republic of China.
[l]School of Physics and Electronics, Hunan University, Changsha 410082, China.
[m]Also at Guangdong Provincial Key Laboratory of Nuclear Science, Institute of Quantum Matter, South China Normal University, Guangzhou 510006, China.

systematic. In combination with the absolute branching fraction $\mathcal{B}(D^+ \to K^+ K_S^0 \pi^0)$ measured by BESIII, we obtain $\mathcal{B}(D^+ \to K^*(892)^+ K_S^0) = (8.69 \pm 0.40 \pm 0.64 \pm 0.51) \times 10^{-3}$, where the third uncertainty is due to the branching fraction $\mathcal{B}(D^+ \to K^+ K_S^0 \pi^0)$. The precision of this result is significantly improved compared to the previous measurement. This result also differs from most of theoretical predictions by about 4σ, which may help to improve the understanding of the dynamics behind.

I. INTRODUCTION

The study of *CP* violation (CPV) in hadron decays is important for the understanding of the matter-antimatter asymmetry in the Universe. In the charmed-meson sector, CPV effects in singly Cabibbo-suppressed (SCS) D-meson decays are usually much larger than those in Cabibbo-favored and doubly Cabibbo-suppressed decays. In 2019, the LHCb collaboration first observed a CPV effect in a combined analysis of $D^0 \to \pi^+\pi^-$ and $D^0 \to K^+K^-$ decays [1]. However, theoretical predictions of this CPV effect suffer from large variations compared to those in the *K* or *B* meson systems, mainly due to the large uncertainty in describing the nonperturbative dynamics in QCD in the charm region [2,3].

In recent years, the branching fractions (BFs) and CPV in the two-body hadronic decays of $D \to PP$ and $D \to VP$ have been studied in different QCD-derived models [4–7], where *P* and *V* denote pseudoscalar and vector mesons, respectively. Generally, these theoretical calculations are in good agreement with experimental results, except for those of the SCS decay $D^+ \to K^*(892)^+ K_S^0$, whose amplitude consists of color-favored tree diagrams, W-annihilation diagrams, and penguin diagrams [7]. The topological diagrams can be found in Fig. 1. The measured and predicted values of $\mathcal{B}(D^+ \to K^*(892)^+ K_S^0)$ are listed in Table I. The E687 Collaboration reported a BF

ratio of $\frac{\mathcal{B}(D^+ \to K^*(892)^+(\to K^+\pi^0)K_S^0)}{\mathcal{B}(D^+ \to K_S^0\pi^+)} = 1.1 \pm 0.3 \pm 0.4$ [8]. This results in $\mathcal{B}(D^+ \to K^*(892)^+ K_S^0) = (17 \pm 8) \times 10^{-3}$ when combined with the world average of $\mathcal{B}(D^+ \to K_S^0\pi^+)$ [9]. Although the predicted values are consistent with the experimental results, the experimental precision needs to be improved. A precise measurement of $\mathcal{B}(D^+ \to K^*(892)^+ K_S^0)$ will provide a more stringent test of the theoretical models and help to deepen our understanding of the dynamics of charmed meson decays. Especially, this will enhance the predictive power on the CPV in charmed meson decays.

In this paper, the first amplitude analysis of the SCS decay $D^+ \to K^+ K_S^0 \pi^0$ is reported, based on a sample of $D^+ D^-$ pairs from e^+e^- collisions at a center-of-mass energy of $\sqrt{s} = 3.773$ GeV corresponding to an integrated luminosity of 2.93 fb^{-1} [10,11] collected with the BESIII detector [12] at the Beijing Electron Positron Collider (BEPCII) [13]. At the energy $\sqrt{s} = 3.773$ GeV, the pairs of $D^+ D^-$ are produced near threshold without any accompanying hadron [14]. Previously, the BESIII Collaboration measured the BF of $D^+ \to K^+ K_S^0 \pi^0$ to be $(5.07 \pm 0.19 \pm 0.23) \times 10^{-3}$ [15]. In combination with the amplitude analysis results presented in this paper, the BF of $D^+ \to K^*(892)^+ K_S^0$ can be determined with much improved precision. Charge conjugation is implied throughout the text.

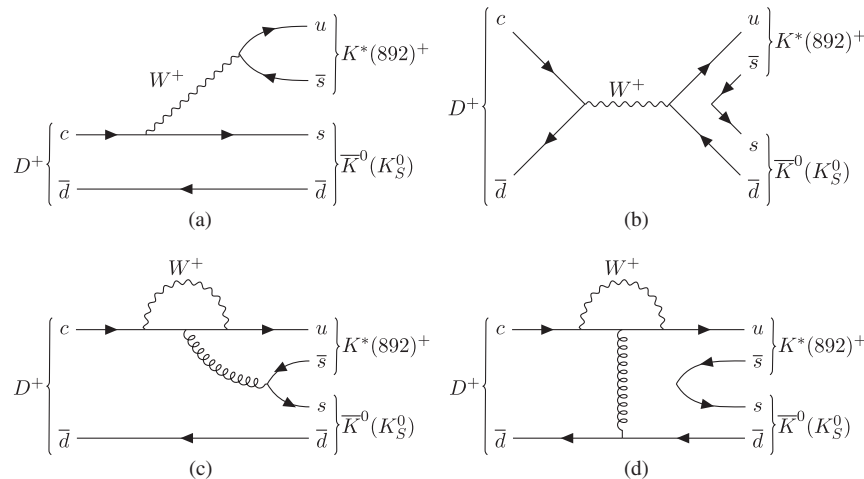FIG. 1. Topological diagrams contributing to the decay $D^+ \to K^*(892)^+ K_S^0$ with (a) color-favored tree diagram, (b) *W*-annihilation diagram, (c) color-favored QCD penguin diagram and (d) QCD penguin exchange diagram.

TABLE I. Predicted BFs of the decay $D^+ \to K^*(892)^+ K_S^0$ from the pole model [4], the factorization-assisted topological-amplitude (FAT) approach with $\rho - \omega$ mixing [5], the topological diagram approach with only tree level amplitude (denoted as TDA[tree] [6], and including QCD-penguin amplitudes (denoted as TDA [QCD-penguin]) [7]. For comparison, the previous experimental result [8,9] is also listed.

Model	$\mathcal{B}(D^+ \to K^*(892)^+ K_S^0)(\times 10^{-3})$
Pole	6.2 ± 1.2
FAT [mix]	5.5
TDA [tree]	5.02 ± 1.31
TDA [QCD-penguin]	4.90 ± 0.21
PDG	17 ± 8

II. BESIII EXPERIMENT AND MONTE CARLO SIMULATION

The BESIII detector records symmetric e^+e^- collisions provided by the BEPCII storage ring, which operates with a peak luminosity of 1×10^{33} cm^{-2} s^{-1} in the center-of-mass energy range from 2.0 to 4.9 GeV. BESIII has collected large data samples in this energy region [2]. The cylindrical core of the BESIII detector covers 93% of the full solid angle and consists of a helium-based multilayer drift chamber (MDC), a plastic scintillator time-of-flight system (TOF), and a CsI(Tl) electromagnetic calorimeter (EMC), which are all enclosed in a superconducting solenoidal magnet providing a 1.0 T magnetic field. The solenoid is supported by an octagonal flux-return yoke with resistive plate counter muon identification modules interleaved with steel. The charged-particle momentum resolution at 1 GeV/c is 0.5%, and the ionization energy loss dE/dx resolution is 6% for electrons from Bhabha scattering. The EMC measures photon energies with a resolution of 2.5% (5%) at 1 GeV in the barrel (end cap) region. The time resolution in the TOF barrel region is 68 ps, while that in the end cap region is 110 ps. More detailed descriptions can be found in Refs. [12,13].

Simulated data samples produced with a GEANT4-based [16] Monte Carlo (MC) package, which includes the geometric description of the BESIII detector [17,18] and the detector response, are used to estimate background contributions and obtain the reconstruction efficiency. The simulation models the beam energy spread and initial state radiation (ISR) in the e^+e^- annihilations with the generator KKMC [19]. The "inclusive MC sample" includes the production of $D\bar{D}$ pairs (including quantum coherence for the neutral D channels), non-$D\bar{D}$ decays of the $\psi(3770)$, ISR production of the J/ψ and $\psi(3686)$ states, and continuum processes which are incorporated in KKMC [19]. Known decay modes are modeled with EvtGen [20] using the BFs published by the Particle Data Group (PDG) [9], and the remaining unknown charmonium decays are modeled with LUNDCHARM [21]. The final state radiation

from charged final state particles is incorporated using PHOTOS [22]. The inclusive MC sample is used to study background contributions and to estimate signal purity. In this work, two sets of signal MC samples are used. One sample is generated with a uniform distribution in phase space (PHSP) for the decay $D^+ \to K^+ K_S^0 \pi^0$, called the "PHSP MC sample," which is used to extract the detection efficiency maps along the Dalitz plot coordinates. The other sample is generated based on the fitted amplitudes from the amplitude analysis, called the "DIY MC sample." It is used to evaluate the fit quality and estimate the systematic uncertainty. The recoiling D^- in these two sets of MC samples is forced to decay into six tag modes, discussed in Sec. III A.

III. EVENT SELECTION

Taking advantage of the threshold production of the D^+D^- sample, this analysis uses a double-tag method, which is illustrated in the following.

A. Tagged candidate selection

The six tag modes used to tag D^- candidates are $K^+\pi^-\pi^-$, $K^+\pi^-\pi^-\pi^0$, $K_S^0\pi^-$, $K_S^0\pi^-\pi^0$, $K_S^0\pi^-\pi^-\pi^+$, and $K^+K^-\pi^-$, with subsequent $\pi^0 \to \gamma\gamma$ and $K_S^0 \to \pi^+\pi^-$ decays. The sum of their BFs is about 27.7% [9]. The tagged candidates are reconstructed from all possible combinations of final state particles according to the following selection criteria.

Charged particle tracks are reconstructed using the information of the MDC, and are required to have a polar angle θ with respect to the z-axis, defined as the symmetry axis of the MDC, satisfying $|\cos\theta| < 0.93$ and to have a distance of closest approach to the interaction point (IP) smaller than 10 cm along the z axis (V_z) and smaller than 1 cm in the perpendicular plane (V_r). Those tracks used in reconstructing $K_S^0 \to \pi^+\pi^-$ decays are exempt from these selection criteria. Particle identification (PID) for charged particle tracks is implemented by using combined information from the flight time measured in the TOF and the dE/dx measured in the MDC to form a PID probability $\mathcal{L}(h)$ for each hadron (h) hypothesis with $h = \pi$, K. Charged tracks are identified as pions when they satisfy $\mathcal{L}(\pi) > \mathcal{L}(K)$ and as kaons otherwise.

Photon candidates from π^0 decays are reconstructed from the electromagnetic showers detected in the EMC crystals. The deposited energy is required to be larger than 25 MeV in the barrel region with $|\cos\theta| < 0.80$ and larger than 50 MeV in the end cap region with $0.86 < |\cos\theta| < 0.92$. To further suppress fake photon candidates due to electronic noise or beam background, the measured EMC time is required to be within 700 ns from the event start time. To reconstruct π^0 candidates, the invariant mass of a photon pair is required to satisfy $0.115 < M_{\gamma\gamma} < 0.150$ GeV/c^2. To further improve the

TABLE II. ΔE_{tag} requirements for different D^- tag modes.

D^- decay	ΔE_{tag} (GeV)
$K^+\pi^-\pi^-$	$(-0.022, 0.021)$
$K^+\pi^-\pi^-\pi^0$	$(-0.060, 0.034)$
$K_S^0\pi^-$	$(-0.019, 0.021)$
$K_S^0\pi^-\pi^0$	$(-0.071, 0.041)$
$K_S^0\pi^-\pi^-\pi^+$	$(-0.025, 0.023)$
$K^+K^-\pi^-$	$(-0.019, 0.018)$

momentum resolution, the invariant mass of the photon pair is constrained to the nominal π^0 mass [9] by applying a one-constraint kinematic fit. The updated momentum of the π^0 is used in the further analysis.

K_S^0 candidates are reconstructed through the decay $K_S^0 \to \pi^+\pi^-$ by combining all pairs of oppositely charged tracks, without applying the PID requirement. These tracks need to satisfy $|\cos\theta| < 0.93$ and $V_z < 20$ cm while no V_r requirement is applied. A vertex fit is applied to pairs of charged tracks constraining them to originate from a common decay vertex, and the χ^2 of this vertex fit is required to be less than 100. The invariant mass of the $\pi^+\pi^-$ pair needs to satisfy $0.487 < M_{\pi^+\pi^-} < 0.511$ GeV/c^2. Here, $M_{\pi^+\pi^-}$ is calculated with the pions constrained to originate at the decay vertex.

To identify the tagged candidates, two kinematic variables, the beam-constrained mass $M_{\text{BC}}^{\text{tag}}$, and the energy difference ΔE_{tag}, are defined as

$$M_{\text{BC}}^{\text{tag}} \equiv \sqrt{E_{\text{beam}}^2/c^4 - |\vec{p}_{\text{tag}}|^2/c^2} \qquad (1)$$

and

$$\Delta E_{\text{tag}} \equiv E_{\text{tag}} - E_{\text{beam}}, \qquad (2)$$

where $\vec{p}_{\text{tag}}$ and E_{tag} are the three-momentum and energy of the tagged D^- candidate in the rest frame of the initial e^+e^- collision system, and E_{beam} is the beam energy. For a correctly reconstructed tagged candidate, $M_{\text{BC}}^{\text{tag}}$ and ΔE_{tag} are expected to be consistent with the nominal D^- mass [9] and zero, respectively. In this work, the same ΔE_{tag} requirements as those in a previous BESIII analysis [23] are used, which are listed in Table II. In each event, only the combination with the smallest $|\Delta E_{\text{tag}}|$ is kept for each tag mode. The tagged candidates are required to be within the region $1.863 < M_{\text{BC}}^{\text{tag}} < 1.879$ GeV/c^2.

B. Signal candidate selection

Signal candidates for $D^+ \to K^+ K_S^0 \pi^0$ are formed using the remaining tracks recoiling against the tagged D^-. Besides the selection requirements for charged and neutral tracks described in Sec. III A, some additional criteria are
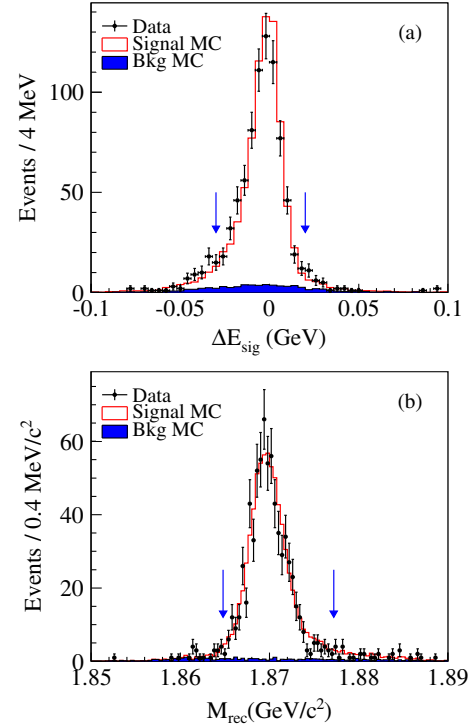

FIG. 2.   Distributions of ΔE_{sig} (a) and M_{rec} (b) in data and the scaled inclusive MC sample. The points with uncertainties denote data and the unshaded (shaded) histogram denotes the signal (background) events from the scaled inclusive MC sample. The arrows indicate the ΔE_{sig} and M_{rec} requirements.

applied to improve the signal-to-background ratio. For the K_S^0 candidates, an additional secondary vertex fit is applied where the momentum of the reconstructed K_S^0 candidate is constrained to be aligned with the direction from the IP to the K_S^0 decay vertex, and the resulting flight length L is required to be larger than twice its uncertainty σ_L. The χ^2 of the secondary vertex fit is required to be less than 500. For the π^0 candidates, the χ^2 of the kinematic fit is required to be less than 20.

To further identify the signal D^+ candidates, the energy difference, ΔE_{sig}, is defined as

$$\Delta E_{\text{sig}} \equiv E_{\text{sig}} - E_{\text{beam}}, \qquad (3)$$

where E_{sig} is the energy of the signal D^+ candidate in the rest frame of the initial e^+e^- collision system. In each event, only the combination with the least $|\Delta E_{\text{sig}}|$ is kept as a signal candidate. The ΔE_{sig} distributions of data and inclusive MC sample are shown in Fig. 2(a). We require $-0.03 < \Delta E_{\text{sig}} < 0.02$ GeV for signal candidates to be kept. To further improve the momentum resolution of the signal final state $K^+ K_S^0 \pi^0$, an additional kinematic fit is applied constraining the invariant mass of the signal final state to the nominal D^+ mass [9] and the total four-momentum of all reconstructed particles to the initial

e^+e^- collision four-momentum. The updated four-momenta are used for further analysis.

The recoil mass M_{rec} is defined as

$$M_{rec} \equiv \sqrt{(\boldsymbol{p}_{e^+e^-} - \boldsymbol{p}_{D^+})^2}/c, \tag{4}$$

where $\boldsymbol{p}_{e^+e^-}$ is the e^+e^- collision initial four-momentum and $\boldsymbol{p}_{D^+}$ is the four-momentum of the D^+ signal candidate. The distribution of M_{rec} in data and in the inclusive MC sample is shown in Fig. 2(b). The candidate events within $1.865 < M_{rec} < 1.877$ GeV/c^2 are selected and the signal purity is determined to be $(97.4 \pm 0.2)\%$ according to the inclusive MC sample. After imposing all above selection criteria, the number of the signal events in data is measured to be 692.

IV. AMPLITUDE ANALYSIS

Only spin-zero particles are involved in the signal process $D^+ \to K^+ K_S^0 \pi^0$; thus, only two degrees of freedom are needed to describe the full kinematics. In the amplitude analysis, we choose the two Dalitz plot variables $M^2_{K^+\pi^0}$ and $M^2_{K_S^0\pi^0}$.

A. Isobar model

The full amplitude of the decay process is described by the Isobar model [24], which is given by

$$\mathcal{M}(D^+ \to K^+ K_S^0 \pi^0) = \sum_i c_i \cdot \mathcal{A}_i, \tag{5}$$

where the term $c_i = a_i e^{i\phi_i}$ consists of the magnitude a_i and the phase ϕ_i for the specific intermediate process i. The amplitude $\mathcal{A}_i$ denotes the decay amplitude of the process i, which is modeled in a quasi-two-body decay $D \to Cr$, $r \to AB$. Here, r is the possible resonance decaying into AB, and A, B, and C each denote one of the final state particles $K^+ K_S^0 \pi^0$. $\mathcal{A}_i$ is formulated as

$$\mathcal{A}_i = F_D \times T_i \times F_r \times W_i, \tag{6}$$

where W_i is the spin factor, F_r and F_D are the Blatt-Weisskopf barrier factors [25], and T_i is the dynamical function describing the intermediate resonance, as illustrated below.

1. Spin factor

The spin factor W_i for the process $D \to Cr$, $r \to AB$ is constructed based on the Zemach formalism [26]. The amplitudes for resonances with angular momenta larger than two are not considered due to the limited phase space. The spin factor is expressed as

Spin-0: $W = 1,$

Spin-1: $W = M^2_{BC} - M^2_{AC} + \dfrac{(M^2_D - M^2_C)(M^2_A - M^2_B)}{M^2_{AB}},$

Spin-2: $W = a_1 - \dfrac{1}{3} a_2 a_3,$ $\qquad$ (7)

where a_1, a_2, and a_3 are given by

$$a_1 = \left[M^2_{BC} - M^2_{AC} + \frac{(M^2_D - M^2_C)(M^2_A - M^2_B)}{M^2_{AB}} \right]^2,$$

$$a_2 = M^2_{AB} - 2M^2_D - 2M^2_C + \frac{(M^2_D - M^2_C)^2}{M^2_{AB}},$$

$$a_3 = M^2_{AB} - 2M^2_A - 2M^2_B + \frac{(M^2_A - M^2_B)^2}{M^2_{AB}}. \tag{8}$$

Here, M_{AB}, M_{AC}, and M_{BC} denote the invariant masses of the particle combinations AB, AC, and BC, respectively, and M_A, M_B, M_C, and M_D denote the nominal masses of A, B, C, and D, respectively.

2. Blatt-Weisskopf barrier factors

The Blatt-Weisskopf barrier factors F_D and F_r attempt to model the underlying quark structure of the parent particle in the decay $D \to rC$ and the subsequent decay $r \to AB$, respectively. The expressions for the barrier factors, which are shown in Table III, are taken from Ref. [25]. In these expressions, p is the decay momentum of the particle A (C) in the rest frame of the mother particle r (D), while q is the decay momentum of the particle A (C) in the rest frame of the mother particle r (D) when the resonance is fixed at the corresponding nominal mass. The radii of D^+ and the intermediate resonance r are chosen as $R_D = 5$ GeV^{-1} and $R_r = 1.5$ GeV^{-1}, respectively [24,27].

3. Dynamical function

The dynamical function describes the line shape of the intermediate resonance. For the specific process $r \to AB$, the dynamical function is chosen as a relativistic Breit-Wigner function for most of the resonances and is written as

TABLE III. Expressions for Blatt-Weisskopf barrier factors [25] under different angular momenta L.

L	F
0	1
1	$\sqrt{\dfrac{1+(R\cdot p)^2}{1+(R\cdot q)^2}}$
2	$\sqrt{\dfrac{9+3(R\cdot p)^2+(R\cdot p)^4}{9+3(R\cdot q)^2+(R\cdot q)^4}}$

$$T(M_{AB}) = \frac{1}{M_r^2 - M_{AB}^2 - iM_r\Gamma(M_{AB})}, \qquad (9)$$

where M_r is the nominal resonance mass, M_{AB} is the invariant mass of AB, and $\Gamma(M_{AB})$ is the mass-dependent width defined as

$$\Gamma(M_{AB}) = \Gamma_r \left(\frac{p_{AB}}{p_r}\right)^{2J+1} \left(\frac{M_r}{M_{AB}}\right) F_r^2, \qquad (10)$$

where Γ_r is the nominal resonance width, J is the spin of the resonance, and p_{AB} and p_r are the breakup momenta at M_{AB} and M_r, respectively.

For the dynamical function of the $K\pi$ $\mathcal{S}$-wave, we choose the large aperture superconducting solenoid (LASS) parametrization [28]. It includes both the $K_0^*(1430)$ resonances and a nonresonant part. We denote the full LASS parametrization as $(K^+\pi^0)_{\mathcal{S}\text{-wave}}$ or $(K_S^0\pi^0)_{\mathcal{S}\text{-wave}}$ in the following. The LASS parametrization can be expressed as

$$T(M_{K\pi}) = \frac{M_{K\pi}}{p_{K\pi}} \cdot \left[F_{K\pi}^{\text{NR}} \cdot \sin(\delta_{K\pi}^{\text{NR}} + \phi_{K\pi}^{\text{NR}}) \cdot e^{i(\delta_{K\pi}^{\text{NR}} + \phi_{K\pi}^{\text{NR}})} \right.$$
$$\left. + F_{K\pi}^{K_0^*} \cdot \sin\delta_{K\pi}^{K_0^*} \cdot e^{i(\delta_{K\pi}^{K_0^*} + \phi_{K\pi}^{K_0^*})} \cdot e^{2i(\delta_{K\pi}^{\text{NR}} + \phi_{K\pi}^{\text{NR}})} \right], \qquad (11)$$

where $F_{K\pi}^{\text{NR}}$ ($\phi_{K\pi}^{\text{NR}}$) and $F_{K\pi}^{K_0^*}$ ($\phi_{K\pi}^{K_0^*}$) are the magnitudes (phases) for the nonresonant and $K_0^*(1430)$ components, respectively, and $p_{K\pi}$ is the breakup momentum of the $K\pi$ system. The phase shifts $\delta_{K\pi}^{\text{NR}}$ and $\delta_{K\pi}^{K_0^*}$ are defined as

$$\delta_{K\pi}^{\text{NR}} = \cot^{-1}\left(\frac{1}{a_{\text{scat}}p_{K\pi}} + \frac{r_{\text{eff}}p_{K\pi}}{2}\right) \qquad (12)$$

and

$$\delta_{K\pi}^{K_0^*} = \tan^{-1}\left[\frac{M_{K_0^*}\Gamma(M_{K\pi})}{M_{K_0^*}^2 - M_{K\pi}^2}\right], \qquad (13)$$

where a_{scat} is the scattering length, r_{eff} is the effective interaction range, and $M_{K_0^*}$ is the nominal mass of the $K_0^*(1430)$. The LASS parametrization corresponds to a K-matrix approach [29] describing a rapid phase shift coming from the resonant term and a slowly rising shift governed by the nonresonant term, with relative strengths $F_{K\pi}^{K_0^*}$ and $F_{K\pi}^{\text{NR}}$. In the nominal fit, the LASS parameters are fixed according to the values measured by the *BABAR* and Belle collaborations [30], which are listed in Table IV.

B. Likelihood function

In the amplitude analysis, a maximum likelihood fit is performed by minimizing the negative log-likelihood (NLL), which is constructed on the Dalitz plot plane as

TABLE IV. Parameters of the $K\pi$ $\mathcal{S}$-wave component measured by *BABAR* and Belle [30].

Parameter	Value	Unit
$M_{K_0^*}$	1.441 ± 0.002	GeV/c^2
$\Gamma_{K_0^*}$	0.193 ± 0.004	GeV
$F_{K\pi}^{\text{NR}}$	0.96 ± 0.07	$\cdots$
$\phi_{K\pi}^{\text{NR}}$	0.1 ± 0.3	deg.
$F_{K\pi}^{K_0^*}$	1 (fixed)	$\cdots$
$\phi_{K\pi}^{K_0^*}$	-109.7 ± 2.6	deg.
a_{scat}	0.113 ± 0.006	$(\text{GeV}/c)^{-1}$
r_{eff}	-33.8 ± 1.8	$(\text{GeV}/c)^{-1}$

$$-\ln\mathcal{L} = -\sum_{\text{events}} \ln\left[\eta(x,y) \cdot \frac{\sum_{i,j}c_i c_j^* \mathcal{A}_i(x,y)\mathcal{A}_j^*(x,y)}{\sum_{i,j}c_i c_j^* I_{ij}}\right], \qquad (14)$$

where (x,y) denote the Dalitz plot coordinates $(M_{K^+\pi^0}^2, M_{K_S^0\pi^0}^2)$, $\eta(x,y)$ is the efficiency function based on the smoothed histogram (following the method in Ref. [31]) from the PHSP MC sample, where the Dalitz plot and the corresponding projections of the PHSP MC are illustrated in Fig. 3, $\mathcal{A}_i(x,y)$ is the decay amplitude of the ith component in Eq. (6), c_i is the free complex coefficient of the ith component, and I_{ij} is the normalization integral, which is defined as

$$I_{ij} = \int \mathcal{A}_i(x,y)\mathcal{A}_j^*(x,y)\eta(x,y)\mathrm{d}x\mathrm{d}y. \qquad (15)$$

Here, the integral is calculated numerically by dividing the Dalitz plot plane into a grid of 3500×3500 square cells. No background contribution is included in the NLL in the nominal fit, exploiting the high signal purity.

C. Fit fraction and goodness-of-fit test

The fit fraction (FF) f_i for the ith component is calculated with

$$f_i = \frac{|c_i|^2 \int |\mathcal{A}_i|^2 \mathrm{d}x\mathrm{d}y}{\sum_{j,k}c_j c_k^* \int \mathcal{A}_j \mathcal{A}_k^* \mathrm{d}x\mathrm{d}y}, \qquad (16)$$

where the integral is calculated using the same numerical method as for the integral in Eq. (15). Note that the sum of the FFs is not necessarily equal to unity due to the interferences between different components. To obtain the corresponding statistical uncertainties, the values of the fitted coefficients c_i are randomly modified for 1000 times according to the information of the covariance matrix and the root-mean-square values of the distributions of the modified FFs are taken as the statistical uncertainties.
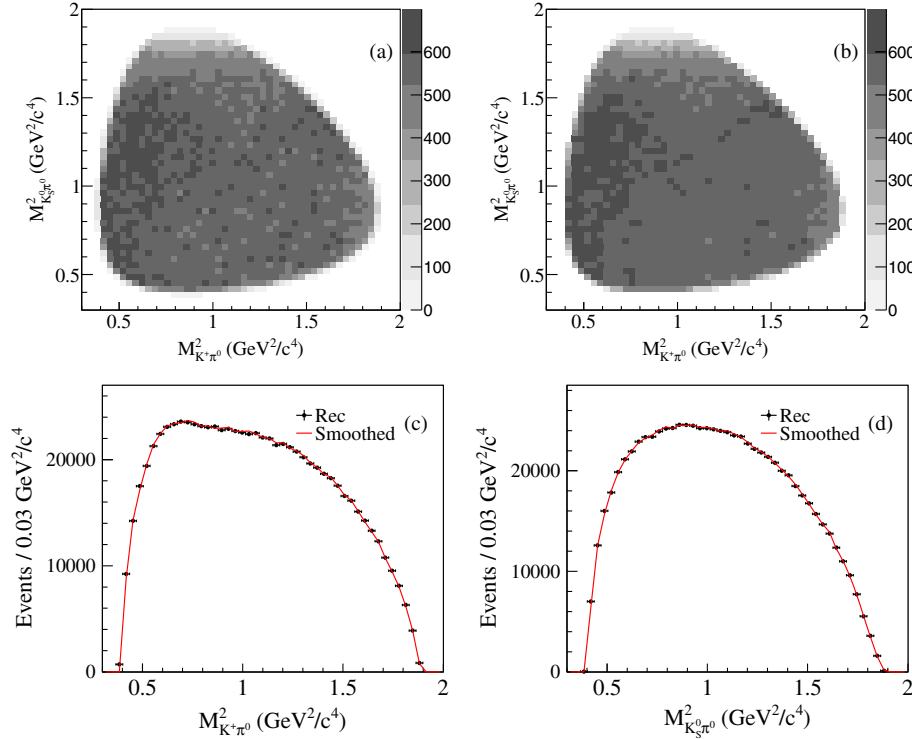
FIG. 3.   Dalitz plot for (a) the reconstructed distribution of the PHSP MC sample and (b) the corresponding smoothed distribution. The projections on (c) $M^2_{K^+\pi^0}$ and (d) $M^2_{K_S^0\pi^0}$, where the dots with uncertainties denote the reconstructed and the solid lines denote the corresponding smoothed distributions.

To examine the quality of the nominal fit, goodness-of-fit tests on three different projections of the Dalitz plot are performed using the fitted results. When calculating χ^2 for each projection, an adaptive binning is adopted to ensure that the minimum number of events is larger than 10 to obey the Gaussian assumption. The χ^2 value is calculated by using the number of events in data n^k_{data} and the expected number n^k_{fitted} from the nominal fit in the kth bin and is formulated as

$$\chi^2 = \sum_k \left(\frac{n^k_{\text{data}} - n^k_{\text{fitted}}}{\sqrt{n^k_{\text{data}}}} \right)^2. \tag{17}$$

V. FIT RESULTS

To perform the amplitude analysis, the open-source framework GooFit [32] is used accelerating the fit speed using parallel processing computing. In the fit, the resonance $K^*(892)^+$ is chosen as the reference, whose phase and magnitude are fixed to be one and zero, respectively. First, the fit of data is performed with the amplitudes containing $K^*(892)^+$ and $\bar{K}^*(892)^0$, which are clearly observed in the corresponding invariant mass spectra. Then, two $\mathcal{S}$-wave $K\pi$ components, $(K^+\pi^0)_{\mathcal{S}\text{-wave}}$ and $(K_S^0\pi^0)_{\mathcal{S}\text{-wave}}$ are included. The statistical significances of

these two components, calculated by the change of the log-likelihood values $\Delta(\text{NLL})$ with and without including the component and taking into account the change of the number of degrees of freedom, are both found to be larger than 5σ. Besides these four components, in addition $K^*(1410)$, $K_2^*(1430)$, $a_0(980)$, $a_0(1450)$, $\rho(1450)$, $\rho(1700)$, and $(K\pi)_{\mathcal{P}\text{-wave}}$ components were also tested, but their statistical significances are all lower than 5σ; thus, they are not included in the nominal fit. Here, the $(K\pi)_{\mathcal{P}\text{-wave}}$ denotes the nonresonant $\mathcal{P}$-wave contribution, which is modeled with the same as vector resonances like $K^*(892)^+$ while the dynamical function is set to be constant.

Finally, the nominal fit includes four components, $K^*(892)^+$, $\bar{K}^*(892)^0$, $(K^+\pi^0)_{\mathcal{S}\text{-wave}}$, and $(K_S^0\pi^0)_{\mathcal{S}\text{-wave}}$. In the fit, the nominal masses and widths of $K^*(892)^+$ and $\bar{K}^*(892)^0$ are fixed at the corresponding PDG [9] values. The obtained results of the magnitudes, phases ϕ, and FFs for the different amplitudes are listed in Table V, where the uncertainties are statistical only. The interference fractions between amplitudes are also listed in Table VI. The process $D^+ \rightarrow K^*(892)^+ K_S^0$ is dominant with a fraction of $(57.1 \pm 2.6)\%$. The comparison of the Dalitz plots between the nominal fit and data, and the projections on $M_{K^+\pi^0}$, $M_{K_S^0\pi^0}$, and $M_{K^+K_S^0}$ are shown in Fig. 4. The goodness-of-fit tests show that the χ^2 values are close to one and the Dalitz plot fit quality is good.

TABLE V. Nominal fit results of magnitudes, phases ϕ, and FFs for different components. The uncertainties are statistical only. The total FF is 80.9%. The statistical significance of each amplitude is also listed.

Amplitude	Magnitude	Phase ϕ (°)	FF (%)	Significance
$D^+ \to K^*(892)^+ K_S^0$	1.0 (fixed)	0.0 (fixed)	57.1 ± 2.6	29.6σ
$D^+ \to \bar{K}^*(892)^0 K^+$	0.41 ± 0.04	162 ± 10	10.2 ± 1.5	11.6σ
$D^+ \to (K^+\pi^0)_{\mathcal{S}\text{-wave}} K_S^0$	2.02 ± 0.37	140 ± 14	3.9 ± 1.5	5.2σ
$D^+ \to (K_S^0\pi^0)_{\mathcal{S}\text{-wave}} K^+$	3.14 ± 0.46	-173.7 ± 9.7	9.7 ± 2.6	7.4σ

TABLE VI. Interference fractions between amplitudes in units of percentage, where A denotes $D^+ \to K^*(892)^+ K_S^0$, B denotes $D^+ \to \bar{K}^*(892)^0 K^+$, C denotes $D^+ \to (K^+\pi^0)_{\mathcal{S}\text{-wave}} K_S^0$, and D denotes $D^+ \to (K_S^0\pi^0)_{\mathcal{S}\text{-wave}} K^+$. The uncertainties are statistical only.

	B	C	D
A	4.8 ± 0.5	0.0 ± 0.0	6.2 ± 0.4
B		2.3 ± 1.5	0.0 ± 0.0
C			5.8 ± 2.6

VI. SYSTEMATIC UNCERTAINTY

The systematic uncertainties for the resonance amplitudes $D^+ \to K^*(892)^+ K_S^0$ and $D^+ \to \bar{K}^*(892)^0 K^+$ are discussed below. While the two $\mathcal{S}$-wave $K\pi$ components are included in our fit in order to improve the fit quality, in general the limited statistics of the data sample does not allow for detailed studies on these contributions so that we limit our systematic studies to the $D^+ \to K^*(892)^+ K_S^0$ and $D^+ \to \bar{K}^*(892)^0 K^+$ results. They are categorized into the following sources: (I) amplitude components, (II) input parameters for resonances, (III) radius of the meson (R_r and R_D), (IV) background, (V) fit bias, and (VI) efficiency. The results of the systematic uncertainties for phases and FFs are summarized in Table VII, where the uncertainties are given in units of the corresponding statistical uncertainties, and the total systematic uncertainties are obtained by summing up all contributions in quadrature under the assumption that different sources are uncorrelated.

(I) *Amplitude components:* To estimate the systematic uncertainties related to the imperfect amplitude components, several ensembles of simulated experiments ("toy MC samples") are generated based on the results of the nominal fit with randomly added additional components
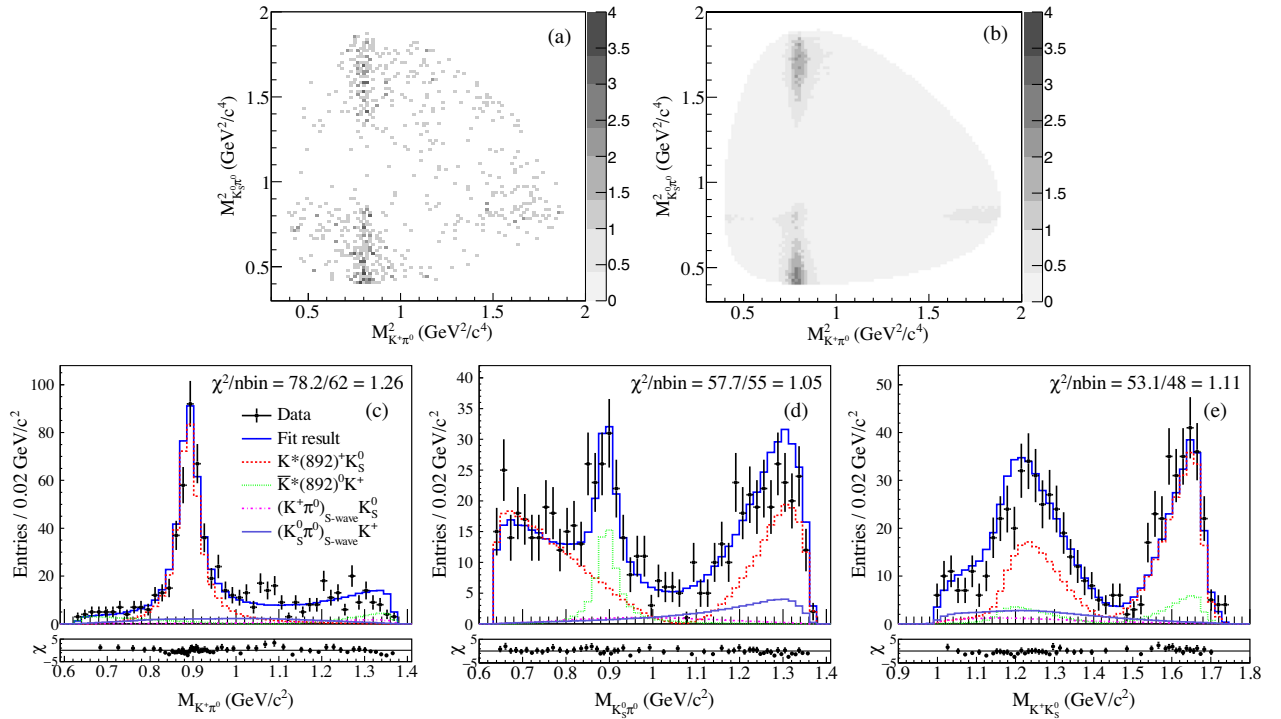

FIG. 4. The Dalitz plot distributions of (a) data and (b) nominal fit, along with the projections and corresponding pull distributions on (c) $M_{K^+\pi^0}$, (d) $M_{K_S^0\pi^0}$, and (e) $M_{K^+K_S^0}$ of the nominal fit, where the black points with error bars denote data, the blue solid lines denote the fit results, and the other colored curves denote the different resonances components.

TABLE VII. Systematic uncertainties on the phases ϕ and FFs for the two resonances $K^*(892)^+$ and $\bar{K}^*(892)^0$ in units of the corresponding statistical uncertainties. The following sources: (I) amplitude components, (II) input parameters for resonances, (III) radius of the meson, (IV) background, (V) fit bias, and (VI) efficiency are considered. The total systematic uncertainties are obtained by summing up all contributions in quadrature.

Source	$D^+ \to K^*(892)^+ K_S^0$	$D^+ \to \bar{K}^*(892)^0 K^+$	
	FF	Phase ϕ	FF
I	1.03	1.03	1.07
II	0.08	0.11	0.12
III	1.13	1.07	1.01
IV	0.01	0.01	0.01
V	0.14	0.05	0.02
VI	0.38	0.05	0.07
Total	1.59	1.49	1.48

from the list $K^*(1410)$, $K_2^*(1430)$, $a_0(980)$, $a_0(1450)$, $\rho(1450)$, $\rho(1700)$, and $(K\pi)_{\mathcal{P}\text{-wave}}$. The magnitude of the additional component is randomly distributed in the range between zero and the fitted magnitude of the $D^+ \to \bar{K}^*(892)^0 K^+$ component, and its phase is randomly distributed in the range $[0, 2\pi)$. Then, the fit procedure is repeated for each toy MC sample. From these fits, we obtain pull distributions for the fit results $\phi_{\bar{K}^*(892)^0}$, $\text{FF}_{K^*(892)^+}$, and $\text{FF}_{\bar{K}^*(892)^0}$ compared to the nominal result that are well described by a Gaussian. The widths of the corresponding Gaussian functions describing the pull distributions are assigned as the associated systematic uncertainties.

(II) *Input parameters:* In the nominal fit, the masses and widths of $K^*(892)^+$ and $\bar{K}^*(892)^0$ are fixed to the values in the PDG [9] and the parameters of the LASS model are fixed according to Ref. [30]. To estimate the corresponding systematic uncertainties, the fit procedure is repeated by varying each of the fixed parameters by $\pm 1\sigma$. The quadratic sum of the maximum relative variations for each parameter is taken as the systematic uncertainty.

(III) *Radii of the mesons:* To estimate the relevant systematic uncertainties originating from fixing the R_D value, the fits are performed with alternative R_D values between 3 and 7 GeV^{-1}. The maximum relative variations of the fit results are taken as the relevant systematic uncertainties. In case of the R_r value, which is one of the dominant sources of systematic uncertainty, toy MC samples are generated based on the fit results with randomly distributed R_r parameters in the range $[0, 3]$ GeV^{-1}. These toy MC samples are then fitted with the R_r parameter fixed to the default value of 1.5 GeV^{-1}. The observed pull distribution can be described by a Gaussian function. The width of the Gaussian function used to fit the pull distribution is taken as systematic uncertainty. The quadratic sum of these two uncertainties is taken as the corresponding systematic uncertainty.

(IV) *Background:* In the nominal fit, the background is neglected due to high signal purity. To estimate the associated systematic uncertainty, the NLL is alternatively constructed as

$$-\ln \mathcal{L} = -\sum_{\text{events}} \ln \left[f \cdot \eta(x, y) \cdot \frac{\sum_{i,j} c_i c_j^* \mathcal{A}_i(x, y) \mathcal{A}_j^*(x, y)}{\sum_{i,j} c_i c_j^* I_{ij}} \right.$$
$$\left. + (1 - f) \cdot B(x, y) \right], \qquad (18)$$

where f is the signal fraction calculated from the M_{rec} distribution in the inclusive MC sample and $B(x, y)$ is the background distribution modeled with a smoothed histogram [31] constructed from the inclusive MC sample. After minimizing the NLL in Eq. (18) with the components of the nominal solution, the relative variation of the fit results is found to be smaller than 1% of the corresponding statistical uncertainty. The variations are assigned as the systematic uncertainties.

(V) *Fit bias:* To understand the potential effect of the fit bias, a series of DIY MC samples with same statistics as in data are generated. The fit procedure is repeated for each DIY MC sample and the pull distributions compared to the nominal fit result are obtained. Any deviation from a mean of zero of the pull distribution is assigned as a systematic uncertainty.

(VI) *Efficiency:* Uncertainties from the efficiencies for charged particle tracking and PID, as well as the reconstruction of K_S^0 and π^0 candidates have been studied with different control samples in previous works; see Refs. [33–35] for examples. To estimate the corresponding systematic uncertainties, we use correction factors comparing the estimated efficiencies in data and MC simulation, $\varepsilon_{\text{Data}}/\varepsilon_{\text{MC}}$, to reweight the efficiency function. We obtain a modified efficiency $\eta'(x, y)$, which is then used instead of $\eta(x, y)$ in Eqs. (14) and (15). The relative variation of the fit results using the modified efficiency is taken as the corresponding systematic uncertainty. Additionally, the systematic uncertainties due to the M_{rec} and ΔE requirements are studied by slightly shifting the boundaries within 1 MeV/c^2 and 1 MeV, respectively. The modified efficiency functions are obtained and the fit procedure is repeated. Finally, the quadratic sum of the above variations is assigned as the systematic uncertainty related to the efficiency.

VII. SUMMARY

To summarize, based on an $e^+ e^-$ collision sample corresponding to an integrated luminosity of 2.93 fb^{-1} collected with the BESIII detector at $\sqrt{s} = 3.773$ GeV, the first amplitude analysis of $D^+ \to K^+ K_S^0 \pi^0$ is carried out. The decay $D^+ \to K^*(892)^+ K_S^0$ is found to be dominant along with a small fraction of $D^+ \to \bar{K}^*(892)^0 K^+$. As listed in Table VIII, the relative BFs

TABLE VIII.   The obtained results based on the amplitude analysis. The subscript stat. and syst. denote statistical and systematic uncertainties, respectively, and Br. denote uncertainties from the quoted BF $\mathcal{B}(D^+ \to K^+ K_S^0 \pi^0)$. For comparison, the previous experimental results [9] are also listed.

BF	This work	PDG
$\frac{\mathcal{B}(D^+ \to K^*(892)^+(K^+\pi^0)K_S^0)}{\mathcal{B}(D^+ \to K^+ K_S^0 \pi^0)}$	$(57.1 \pm 2.6_{\text{stat}} \pm 4.2_{\text{syst}})\%$	$\cdots$
$\frac{\mathcal{B}(D^+ \to \bar{K}^*(892)^0(K_S^0\pi^0)K^+)}{\mathcal{B}(D^+ \to K^+ K_S^0 \pi^0)}$	$(10.2 \pm 1.5_{\text{stat}} \pm 2.2_{\text{syst}})\%$	$\cdots$
$\mathcal{B}(D^+ \to K^*(892)^+ K_S^0)$	$(8.69 \pm 0.40_{\text{stat}} \pm 0.64_{\text{syst}} \pm 0.51_{\text{Br}}) \times 10^{-3}$	$(17 \pm 8) \times 10^{-3}$
$\mathcal{B}(D^+ \to \bar{K}^*(892)^0 K^+)$	$(3.10 \pm 0.46_{\text{stat}} \pm 0.68_{\text{syst}} \pm 0.18_{\text{Br}}) \times 10^{-3}$	$(3.74^{+0.12}_{-0.20}) \times 10^{-3}$

are measured to be $\frac{\mathcal{B}(D^+ \to K^*(892)^+(K^+\pi^0)K_S^0)}{\mathcal{B}(D^+ \to K^+ K_S^0 \pi^0)} = (57.1 \pm 2.6 \pm 4.2)\%$ and $\frac{\mathcal{B}(D^+ \to \bar{K}^*(892)^0(K_S^0\pi^0)K^+)}{\mathcal{B}(D^+ \to K^+ K_S^0 \pi^0)} = (10.2 \pm 1.5 \pm 2.2)\%$, where the first uncertainty is statistical and the second systematic. Using $\mathcal{B}(D^+ \to K^+ K_S^0 \pi^0) = (5.07 \pm 0.19 \pm 0.23) \times 10^{-3}$, as measured by the BESIII Collaboration [15], $\mathcal{B}(D^+ \to K^*(892)^+ K_S^0) = (8.69 \pm 0.40 \pm 0.64 \pm 0.51) \times 10^{-3}$ is obtained, where the third uncertainty is due to the uncertainty on $\mathcal{B}(D^+ \to K^+ K_S^0 \pi^0)$. This result is consistent with previous results [8,9] but with a precision improved by a factor of 4.6. It differs from the theoretical predictions in Refs. [5–7] by about 4σ. However, the result is consistent with the prediction based on the pole model [4], which suffers from large theoretical uncertainty. This indicates that the QCD-derived models need further improvements, which may lead to variations in the predicted CPV effects. In addition, $\mathcal{B}(D^+ \to \bar{K}^*(892)^0 K^+) = (3.10 \pm 0.46 \pm 0.68 \pm 0.18) \times 10^{-3}$ is obtained, which agrees well with previous measurements [9] and theoretical predictions [4–7]. Future $\psi(3770)$ data samples at BESIII with larger statistics will provide more precise information about the process $D^+ \to K^*(892)^+ K_S^0$ and help to deepen our understanding of the internal dynamics of charmed meson decays [2].

ACKNOWLEDGMENTS

[1] R. Aaij *et al.* (LHCb Collaboration), Phys. Rev. Lett. **122,** 211803 (2019).

[2] M. Ablikim *et al.* (BESIII Collaboration), Chin. Phys. C **44,** 040001 (2020).

[3] M. Saur and F. S. Yu, Sci. Bull. **65,** 1428 (2020).

[4] F. S. Yu, X. X. Wang, and C. D. Lyu, Phys. Rev. D **84,** 074019 (2011).

[5] Q. Qin, H. N. Li, C. D. Lyu, and F. S. Yu, Phys. Rev. D **89,** 054006 (2014).

[6] H. Y. Cheng, C. W. Chiang, and A. L. Kuo, Phys. Rev. D **93,** 114010 (2016).

[7] H. Y. Cheng and C. W. Chiang, Phys. Rev. D **100,** 093002 (2019).

[8] P. L. Frabetti *et al.* (E687 Collaboration), Phys. Lett. B **346,** 199 (1995).

[9] P. A. Zyla *et al.* (Particle Data Group), Prog. Theor. Exp. Phys. **2020,** 083C01 (2020).

[10] M. Ablikim *et al.* (BESIII Collaboration), Chin. Phys. C **37,** 123001 (2013).

[11] M. Ablikim *et al.* (BESIII Collaboration), Phys. Lett. B **753,** 629 (2016).

[12] M. Ablikim *et al.* (BESIII Collaboration), Nucl. Instrum. Methods Phys. Res., Sect. A **614,** 345 (2010).

[13] C. H. Yu *et al.*, in *Proceedings of IPAC2016, Busan, Korea, 2016* (JACoW, Geneva, 2016), https://doi.org/10.18429/JACoW-IPAC2016-TUYA01.

[14] H. B. Li and X. R. Lyu, arXiv:2103.00908.

[15] M. Ablikim *et al.* (BESIII Collaboration), Phys. Rev. D **99,** 032002 (2019).

[16] S. Agostinelli *et al.* (GEANT Collaboration), Nucl. Instrum. Methods Phys. Res., Sect. A **506,** 250 (2003).

[17] Z. Y. You, Y. T. Liang, and Y. J. Mao, Chin. Phys. C **32,** 572 (2008).

[18] Y. T. Liang, B. Zhu, and Z. Y. You *et al.*, Nucl. Instrum. Methods Phys. Res., Sect. A **603,** 325 (2009).

[19] S. Jadach, B. F. L. Ward, and Z. Was, Phys. Rev. D **63,** 113009 (2001); Comput. Phys. Commun. **130,** 260 (2000).

[20] D. J. Lange, Nucl. Instrum. Methods Phys. Res., Sect. A **462,** 152 (2001); R. G. Ping, Chin. Phys. C **32,** 599 (2008).

[21] J. C. Chen, G. S. Huang, X. R. Qi, D. H. Zhang, and Y. S. Zhu, Phys. Rev. D **62,** 034003 (2000).

[22] E. Richter-Was, Phys. Lett. B **303,** 163 (1993).

[23] M. Ablikim *et al.* (BESIII Collaboration), Phys. Rev. D **97,** 072015 (2018).

[24] H. Albrecht *et al.* (ARGUS Collaboration), Phys. Lett. B **308,** 435 (1993).

[25] F. v. Hippel and C. Quigg, Phys. Rev. D **5,** 624 (1972).

[26] C. Zemach, Phys. Rev. **140,** B109 (1965).

[27] S. Kopp *et al.* (CLEO Collaboration), Phys. Rev. D **63,** 092001 (2001).

[28] D. Aston *et al.*, Nucl. Phys. **B296,** 493 (1988).

[29] I. J. R. Aitchison, Nucl. Phys. **A189,** 417 (1972).

[30] I. Adachi *et al.* (*BABAR* and Belle Collaborations), Phys. Rev. D **98,** 112012 (2018).

[31] J. Friedman, in *Proceedings of the 1974 CERN School of Computing, Godøysund, Norway, 1974* (CERN, Geneva, 1974).

[32] R. Andreassen *et al.*, IEEE Access **2,** 160 (2014).

[33] M. Ablikim *et al.* (BESIII Collaboration), Phys. Rev. D **89,** 052001 (2014).

[34] M. Ablikim *et al.* (BESIII Collaboration), Phys. Rev. D **96,** 012002 (2017).

[35] M. Ablikim *et al.* (BESIII Collaboration), Phys. Rev. Lett. **126,** 092002 (2021).